

The double RGB in M 2: C, N, Sr and Ba abundances^{*}

C. Lardo^{1†}, E. Pancino^{1,2}, A. Mucciarelli³, M. Bellazzini¹, M. Rejkuba^{4,5},
S. Marinoni^{2,6}, G. Cocozza¹, G. Altavilla¹ and S. Ragaini¹

¹ *INAF-Osservatorio Astronomico di Bologna, Via Ranzani 1, I-40127 Bologna, Italy*

² *ASI Science Data Center, I-00044, Frascati, Italy*

³ *Department of Physics and Astronomy, University of Bologna, Viale Berti Pichat 6/2, I-40127 Bologna, Italy*

⁴ *ESO, Karl-Schwarzschild-Strasse 2, 85748 Garching b. München, Germany*

⁵ *Excellence Cluster Universe, Boltzmannstr. 2, D-85748, Garching, Germany*

⁶ *INAF-Osservatorio Astronomico di Roma, via Frascati 33, I-00040, Monte Porzio Catone (RM), Italy*

Accepted 2013 May 14. Received 2013 May 14; in original form 2013 April 5

ABSTRACT

The globular cluster M 2 has a photometrically detected double red giant branch (RGB) sequence. We investigate here the chemical differences between the two RGBs in order to gain insight in the star formation history of this cluster. The low-resolution spectra, covering the blue spectral range, were collected with the MODS spectrograph on the LBT, and analyzed via spectrum synthesis technique. The high quality of the spectra allows us to measure C, N, Ba, and Sr abundances relative to iron for 15 RGB stars distributed along the two sequences. We add to the MODS sample C and N measurements for 35 additional stars belonging to the blue RGB sequence, presented in Lardo et al. (2012). We find a clear separation between the two groups of stars in *s*-process elements as well as C and N content. Both groups display a C-N anti-correlation and the red RGB stars are on average richer in C and N with respect to the blue RGB. Our results reinforce the suggestion that M2 belongs to the family of globular clusters with complex star formation history, together with ω Cen, NGC 1851, and M 22.

Key words:

1 INTRODUCTION

The discovery of photometric multiple evolutionary sequences in Galactic Globular clusters (GCs) color-magnitude diagrams (CMDs) and the presence of distinctive anti-correlations also among unevolved stars has conclusively shown that these systems host at least two generations of stars (see Gratton et al. 2012 and references therein for a discussion). From a chemical perspective, GCs show a

large internal variation in the abundances of light elements (Li, C, N, O, F, Na, Mg, and Al; i.e., Kraft 1994, Gratton et al. 2004, Carretta et al. 2010a, Martell & Smith 2009, Kayser et al. 2008, Pancino et al. 2010, Gratton et al. 2012). On the contrary, the abundances of heavier α (Si, Ca, Ti), iron-peak (Fe, Ni, Cu), and neutron-capture elements (Ba, La, Eu) only rarely show similar star-to-star variation. Besides the remarkable exception of ω Centauri and Terzan 5 (see Johnson & Pilachowski 2010, Ferraro et al. 2009, and references therein), variations in the heavy element content have been detected only for few clusters (e.g., Sneden et al. 1997; Marino et al. 2011; Yong & Grundahl 2008; Villanova et al. 2010; Carretta et al. 2010b and references therein).

M 2 (=NGC 7089) is an intermediate metallicity ([Fe/H] = -1.62; Armandroff & Zinn 1988) GC located in the Galactic halo. Its integrated *V* magnitude ($M_V = -9.02$, Mackey & van den Bergh 2005) puts it among the twelve most luminous clusters in our Galaxy. As other massive GCs, M 2 shows a peculiar horizontal branch morphology (HB) with a long blue tail (see for example Figure 3 of D'Allesandro et al. 2009), possibly indicative of significant he-

^{*} This paper used data obtained with the MODS spectrographs built with funding from NSF grant AST-9987045 and the NSF Telescope System Instrumentation Program (TSIP), with additional funds from the Ohio Board of Regents and the Ohio State University Office of Research. The LBT is an international collaboration among institutions in the United States, Italy and Germany. LBT Corporation partners are: The University of Arizona on behalf of the Arizona university system; Istituto Nazionale di Astrofisica, Italy; LBT Beteiligungsgesellschaft, Germany, representing the Max-Planck Society, the Astrophysical Institute Potsdam, and Heidelberg University; The Ohio State University, and The Research Corporation, on behalf of The University of Notre Dame, University of Minnesota, and University of Virginia.

[†] E-mail: carmela.lardo2@unibo.it

lium variations¹ (see D’Antona et al. 2002, D’Antona et al. 2005, Dalessandro et al. 2013, and references therein) and a split SGB (Piotto et al. 2012).

So far only a few spectroscopic studies have been dedicated to M 2 stars. Armandroff & Zinn (1988) reported a metallicity $[\text{Fe}/\text{H}] = -1.62$ from integrated-light spectroscopy in the region of the Ca II infrared triplet. Smith & Mateo (1990) found M 2 to have a bimodal CN distribution, with the majority of red giants found to be CN-strong stars (but see also earlier results by McClure & Hesser 1981 and Canterna et al. 1982). M 2 also contains two CH stars (Zinn 1981; Smith & Mateo 1990), that are relatively rare within GCs (e.g., Harding 1962, Bond 1975, McClure & Norris 1977, Hesser et al. 1982, Smith & Norris 1982, Cote et al. 1997, Sharina et al. 2012). Smolinski et al. (2011) found that the signs of nitrogen enrichment are present well before the point of first dredge-up.

In Lardo et al. (2011) we were able to detect a spread in light-element abundances of M 2 RGB stars using Sloan u, g, r photometry. In order to measure the exact content of the C and N of RGB stars, we obtained a number of spectra of giants with the DOLORES spectrograph² (Lardo et al. 2012b, hereafter L12). We derived C and N abundances from low-resolution blue spectra of 35 giants with magnitude $17.5 \leq V \leq 14.5$ mag, and found that the carbon and nitrogen abundances are anticorrelated, with a hint of bimodality in the C content for stars with luminosities below the RGB bump ($V \simeq 15.7$ mag), while the range of variations in N abundances is very large and spans almost ~ 2 dex. More interestingly, using U and V images taken during the same observing run, we discovered an anomalous sequence in the CMD of M 2. This feature appears as a narrow, poorly populated RGB, which extends down to the sub giant branch region. In L12 we speculated that this red RGB could be the extension of the faint component of the split SGB recently discovered by Piotto et al. (2012). Unfortunately, no spectra were obtained at that time for stars in this previously unknown substructure.

In this paper we try to fill this gap and present a chemical abundance analysis of a sample of 15 stars distributed along the double RGB of M 2. For clarity, in the following we call B-RGB the bluer sequence containing the bulk of the RGB population of the cluster, and R-RGB the sparse redder sequence identified for the first time in L12.

This article is structured as follows: we describe the sample in Section 2; we outline our measurements of the CN and CH indices and their interpretation in Section 3; we derive C, N, Ba and Sr abundances from spectral synthesis in Section 4 and discuss the result in Section 5. Finally we present a summary of our results and draw conclusions in Section 6.

2 OBSERVATIONS AND DATA REDUCTION

A careful target selection was made for this study. In order to compare in a homogeneous manner abundances of B-RGB stars with those of stars located on the R-RGB, we obtained spectra on both RGBs.

These objects have magnitude $14 \leq V \leq 17$ mag and are present both below and above the bump in the RGB luminosity function (see L12 and Sect. 5.3 for a discussion on the changes on the C and N abundances along the RGB evolution). In particular, we selected M 2 spectroscopic targets from UV photometry presented in L12. The initial sample of candidate stars consisted of those located more than $1'$ and less than $4.5'$ from the center of M 2 to facilitate sky subtraction and reduce fore/background contamination, respectively. Spectroscopic targets were hence chosen as the most isolated stars³ to avoid the contamination of the spectra from other sources.

The observations were secured with MODS, the low- to medium-resolution Multi-Object CCD Spectrograph operating at the twin 8.4-meter diameter mirror Large Binocular Telescope (LBT) on Mt. Graham in southeastern Arizona⁴. MODS allows to allocate slitlets over a $6' \times 6'$ field of view (FoV). We defined one slit mask using the stand-alone version of the Multi-Slit Mask Design Software, provided by the telescope staff⁵. Spectra for RGB stars were obtained with the 400 line mm^{-1} reflection grating⁶, covering a wavelength range of 3200–5800 Å and their resolution was $R \simeq 800, 950, \text{ and } 1030$ at 3360, 4000, and 4300 Å, respectively. The slit width on the masks was fixed to $1.0''$, and the slit length was chosen to be at least $12''$ to allow for local sky subtraction. In order to reach high S/N ratio, the mask configuration was observed three times with exposure durations of 1200 s each, leading to a total exposure time of 1.0 hr and a typical S/N ratio of $\simeq 50\text{--}60$ at 4000 Å. Spectra extraction and wavelength calibration were performed by the Italian LBT Spectroscopic Reduction Center⁷ with a dedicated pipeline. An example of the spectra quality can be found in Figure 1, where some of the regions of interest for the present analysis are shown.

2.1 Membership

To derive the radial velocity of candidate RGB stars, we first performed a cross-correlation of the object spectra with the highest S/N star on each MOS mask as a template with the IRAF routine *fxcor*, as in L12. The radial velocity of the template star was computed using the laboratory positions of several spectral features (e.g., H_α , H_β , H_γ , H_δ , and CaII (H+K)). The measured velocities are plotted as a function of radial distance from the cluster center in Figure 2 and listed in Table 1⁸. The median velocity of -6.7 ± 8.5 km/s for the entire sample is shown as a dashed line. This value,

¹ Star-to-star helium abundance variations are expected as the N-Na anomalies are synthesized during hydrogen burning.

² DOLORES (Device Optimized for the LOW RESolution) is a low resolution spectrograph and camera permanently installed at the Nasmyth B focus of the Telescopio Nazionale Galileo (TNG), located in La Palma, Canary Islands, Spain.

³ Only stars of magnitude V_0 lacking neighbors brighter than $V_0 + 2.0$ within $2''$ of their center were kept in the final target list.

⁴ <http://www.astronomy.ohio-state.edu/MODS/>

⁵ <http://www.astronomy.ohio-state.edu/~martini/mms/>

⁶ With a dispersion of $0.120''/\text{pix}$.

⁷ <http://lbt-spectro.iasf-milano.inaf.it>

⁸ For completeness, we report in this Table also the stars judged cluster non-members based on their radial velocity.

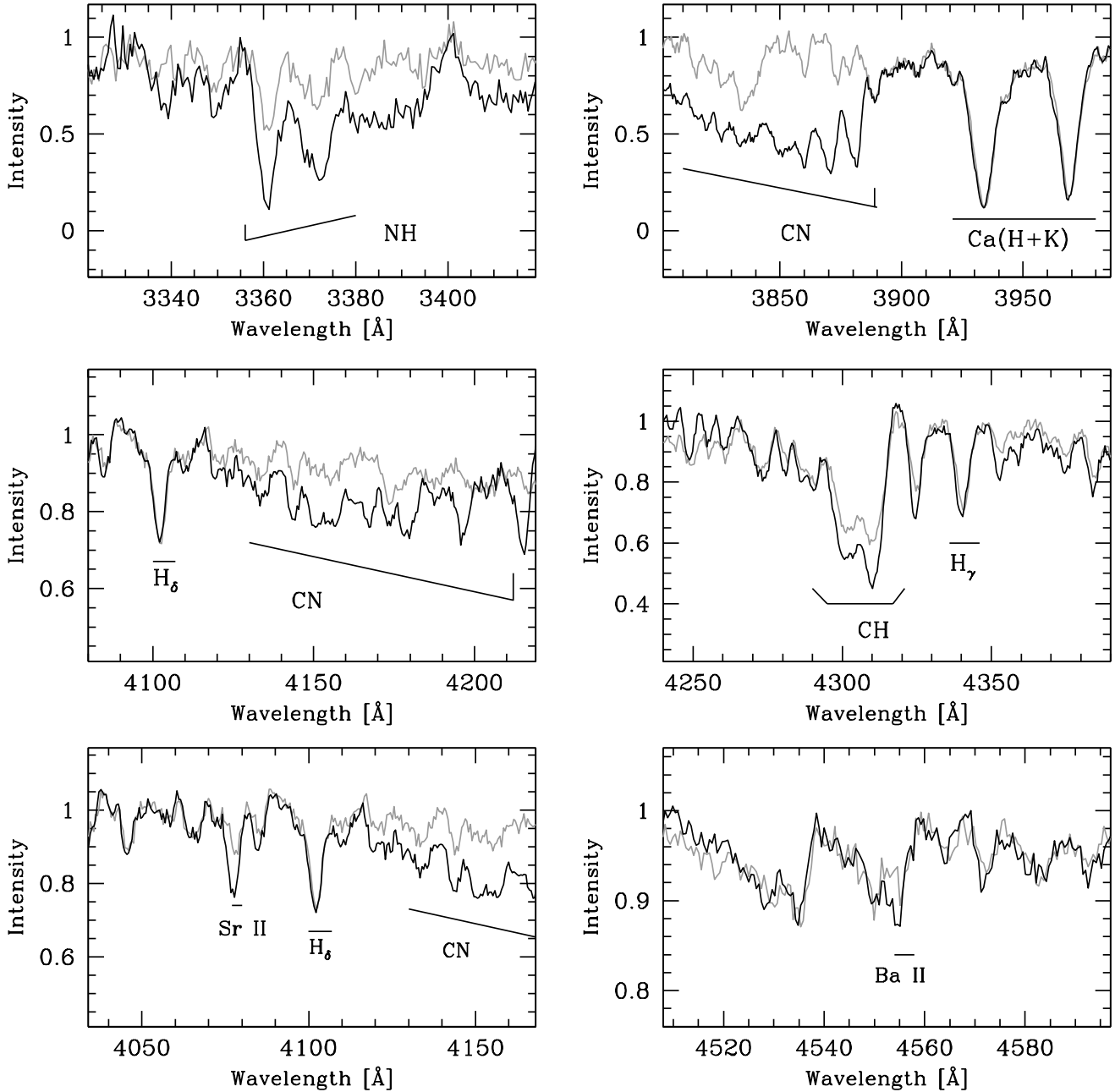


Figure 1. From left to right, top to bottom: comparison of the spectra of NH (at ~ 3360 Å), CN (at ~ 3883 Å and ~ 4200 Å) and CH (at 4300 Å) bands, Sr II lines (4077 Å) and Ba II (4554 Å) in two blue and red RGB stars with similar atmospheric parameters. The spectrum in black is that of the R-RGB star 05569 (with $T_{eff} = 5139$ K and $\log g = 2.5$), and the one in gray is that of the B-RGB star 04837 (with $T_{eff} = 5172$ K and $\log g = 2.5$).

given the low resolution of our spectra, agrees quite well with the value tabulated (-5.0 km/s) in the Harris 1996 (2010 edition) catalog. Then, we rejected individual stars with values deviating by more than 3σ from this average velocity, deeming them to be probable field stars. Three stars (triangles in Figure 2) were rejected using this criterium. To obtain additional membership information we employed the strength of the CaII H and K and H_{β} lines, as a further discriminant between cluster and field star (see also L12 and Section 3).

We noted that one more star (located at the blue edge

of the RGB sequence) had discrepant CaII (H+K) and H_{β} with respect to the bulk of M 2 stars and rejected it from following analysis.

Yet, since the radial velocity of M 2 stars is near to zero, field stars could easily have such velocities. As extensively discussed in L12 (see Section 6), we expect a very small degree of contamination given the relatively high galactic latitude of the cluster (i.e.; $l, b = 53^{\circ}, -36^{\circ}$) and the small FoV considered to select target stars (see Section 2). In L12 we used TRILEGAL (Girardi et al. 2005) and determined that the fraction of Galactic field stars with color $0.4 \leq U - V \leq$

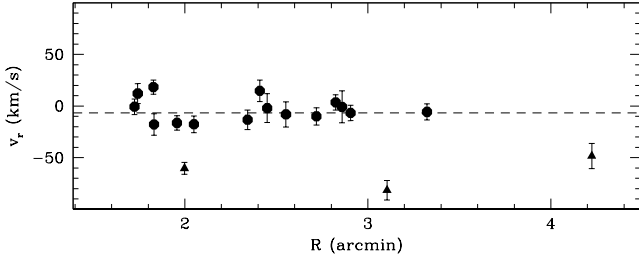


Figure 2. Radial velocity plotted against distance from the cluster center for the stars in our sample. The dashed line is the cluster median velocity of -6.7 km/s. Triangles refer to stars which are not members of M 2, according to their radial velocity.

2.0, magnitude $18.5 \leq V \leq 14.5$ mag, and distance from the cluster center $1' \leq R \leq 4'$ is lower than 1%. For this work we used both TRILEGAL and the Besançon model (Robin et al. 2003)⁹, to obtain a conservative estimate of the degree of contamination affecting our spectroscopic sample¹⁰. We found only 2 (TRILEGAL) or 4 (Besançon)¹¹ stars field stars in with $U - V$ color and V magnitude comparable with those analyzed in this paper. All these stars are relatively metal rich dwarfs ($\log g \geq 4$ dex). According to TRILEGAL, their metallicity ranges from $[\text{Fe}/\text{H}] = -0.61$ dex up to $[\text{Fe}/\text{H}] = -0.13$ dex, while the Besançon model gives a range in metallicity between $[\text{Fe}/\text{H}] = -0.92$ and $[\text{Fe}/\text{H}] = 0.13$ dex. Thus our moderate-resolution spectra are in themselves capable of confirming membership. The spectra of stars rejected on the basis of their radial velocity unambiguously indicates that two of these stars display absorption features very different from those shown by the cluster members and much stronger than expected for the cluster low metallicity (i.e., $[\text{Fe}/\text{H}] = -1.62$ dex). One star appears to have metallicity comparable to those of cluster members, although the measured radial velocity seems to exclude this. Consequently, indices and C and N abundances were not measured for it. To conclude, we note that the stellar spectra shown in Figure 1 are essentially identical everywhere – and this is in particular true for the Ca(H+K) lines – but in the NH, CN, and CH absorption regions. This strongly supports the fact that red-RGB stars are indeed M 2 members.

3 SPECTRAL INDICES

As a preliminary step, we measured a set of indices quantifying the strength of the UV CN band and the G band of CH, the CaII H and K, and H_β lines. We adopted the same indices as defined in Pancino et al. (2010) and L12. The uncertainties related to the index measure have been obtained as in L12 with the expression derived by Vollmann & Eversberg (2006), assuming pure photon noise statistics in the flux measurements.

The measured indices are plotted in Figure 3 versus

⁹ <http://model.obs-besancon.fr/>

¹⁰ For this test we considered only stars with $0.7 \leq (U - V) \leq 2.7$ and $17.0 \leq V \leq 14.0$ mag.

¹¹ We note that only 3 out of 4 stars have velocities comparable to M 2 heliocentric radial velocity.

V magnitude, which shows also the L12 stars for comparison. The two stars above the RGB bump are significantly affected by internal mixing and are discussed separately in Section 5.3. The indices, together with additional information on target stars, are listed in Table 1.

A visual inspection of the Figure 3 (b) and (c) panels reveals that the stars in the R-RGB sequence have both higher S($\lambda 3839$) and CH($\lambda 4300$) than stars in the B-RGB. The difference in S($\lambda 3839$) between CN-strong and CN-weak stars below the bump is $\Delta S(\lambda 3839) \simeq 0.2$ mag, while the measurement error is only of the order of $\simeq 0.03$ mag. The Figure 3 panel (c) shows a plot of the CH($\lambda 4300$) index vs. the V magnitude and illustrates the relation between the CN and CH band strengths for all giants. In this case the index value spread among the measured stars is very small and in any case within the uncertainties.

Because the visual appearance of the MODS spectra suggests enhanced lines of both SrII (4077 Å) and BaII (4554 Å) – see also Figure 1, we measured indices also for these elements¹². The definition of the band passes is the same as in Stanford et al. (2007). The corresponding indices with median error measurements are shown in the panels (d) and (e) of Figure 3. Studying the two plots, one can see that R-RGB stars have, in general, considerably larger index values for both SrII(4077 Å) and BaII(4554 Å) with respect to the B-RGB stars, indicating that stars belonging to the R-RGB are enhanced most probably in s -process element content relatively to the B-RGB stars (see also Figure 1). We refer the reader to Section 5.4 for further discussion on this.

4 ABUNDANCE ANALYSIS

To obtain a quantitative estimate of the detected enhancements in carbon, nitrogen and strontium for R-RGB stars, we derived $[\text{C}/\text{Fe}]$, $[\text{N}/\text{Fe}]$, $[\text{Sr}/\text{Fe}]$, and $[\text{Ba}/\text{Fe}]$ abundance ratios for all MODS stars via spectral synthesis.

4.1 Atmospheric parameters

Stellar parameters were derived from photometry, in the same fashion as described in L12. Briefly, the effective temperature, T_{eff} , was calculated using the Alonso et al. (1999) T_{eff} -color calibrations for giant stars. We used the $(U - V)$ color from DOLORES photometry (once calibrated on Stetson standard field), using $E(B - V) = 0.06$ and $[\text{Fe}/\text{H}] = -1.65$ from the Harris (1996) catalog (2010 edition). In addition, we used — when available — $(B - V)$, $(V - J)$, $(V - H)$, and $(V - K)$ colors from Lee & Carney (1999) and the 2MASS photometry¹³. The final T_{eff} was the mean of the individual T_{eff} values from each color, weighted by the uncertainties of each color calibration. The surface gravity was determined using T_{eff} , a distance modulus of $(m - M)_V = 16.05$ (Harris 1996), bolometric corrections $BC(V)$ from Alonso et al. (1999) and assuming a mass of $0.8 M_\odot$ (Bergbusch &

¹² The higher resolution of MODS data allows for this, while we cannot provide meaningful index measurements for the DOLORES sample.

¹³ [protecthttp://www.ipac.caltech.edu/2mass/overview/access.html](http://www.ipac.caltech.edu/2mass/overview/access.html)

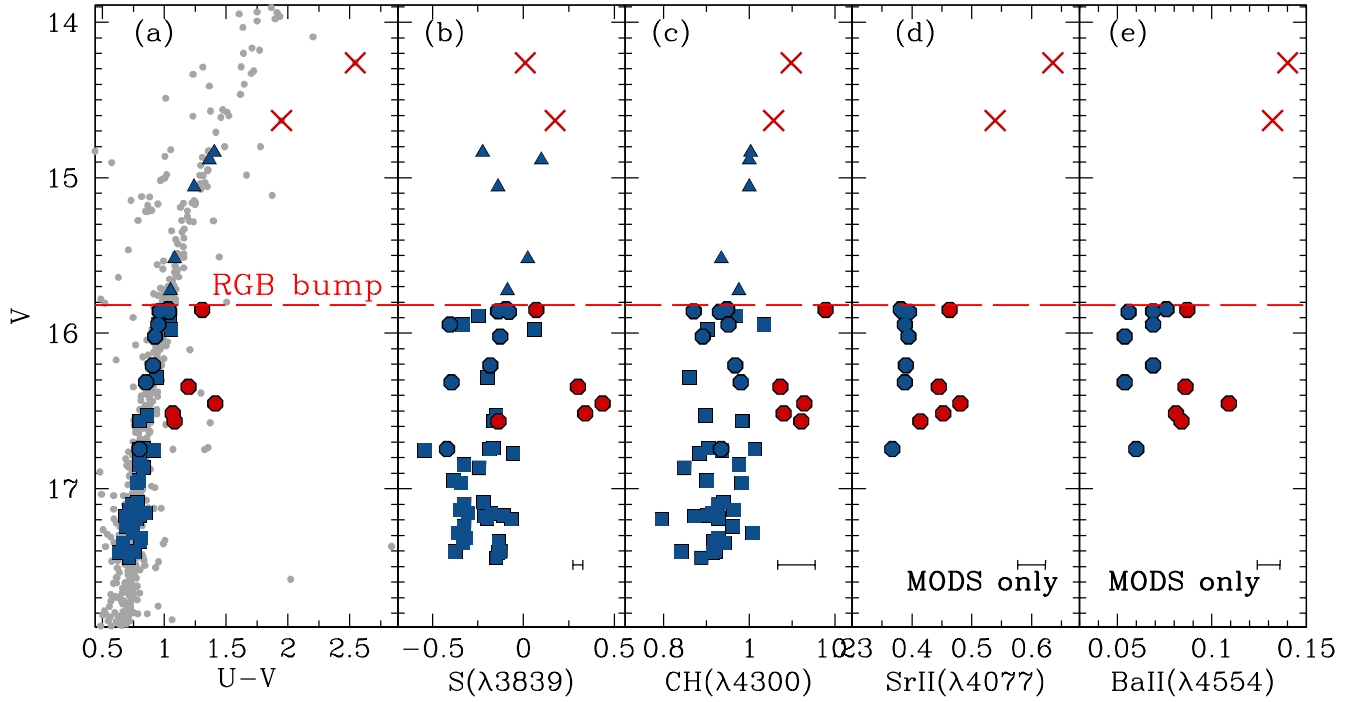


Figure 3. In the (a) panel we present the $V, U - V$ CMD for M 2 from DOLORES images (L12). Squares are the stars presented in L12, while circles refer to the stars analyzed in this work. Stars belonging to the B- and R-RGB are shown in blue and red color, respectively. The location of the RGB bump is indicated by the horizontal dashed line. Stars with luminosities brighter than the RGB bump are plotted as crosses (MODS sample) and triangles (DOLORES spectra). The same symbols and colors are used consistently throughout the whole paper. The (b), (c), (d), and (e) panels present the $S(\lambda 3839)$, $CH(\lambda 4300)$, $SrII(\lambda 4077)$, and $BaII(\lambda 4554)$ indices plotted against stellar V magnitude (with typical measurement error in the bottom right corner), respectively.

Table 1. Sample stars' properties and index measures.

ID ^a	RGB ^b	RA (J200)	DEC (J200)	V (mag)	V_r (km/s)	eV_r (km/s)	CN (mag)	eCN (mag)	CH (mag)	eCH (mag)	SrII (mag)	$eSrII$ (mag)	BaII (mag)	$eBaII$ (mag)
05569	R	21:33:21.25	-00:50:57.23	16.516	-8.1	12.2	0.341	0.029	1.080	0.039	0.452	0.023	0.081	0.006
06893	R	21:33:24.23	-00:50:33.21	16.566	-0.7	7.5	-0.137	0.022	1.121	0.044	0.414	0.023	0.084	0.006
08017	R	21:33:20.09	-00:50:13.29	15.850	-2.1	14.0	0.071	0.019	1.178	0.044	0.463	0.023	0.087	0.006
08984	R	21:33:18.22	-00:49:56.10	14.633	3.5	7.5	0.175	0.029	1.057	0.044	0.539	0.024	0.132	0.006
10130	R	21:33:19.70	-00:49:36.08	16.452	14.7	10.5	0.436	0.035	1.128	0.045	0.481	0.024	0.109	0.006
14911	R	21:33:23.11	-00:48:11.07	14.261	-16.4	7.0	0.011	0.033	1.098	0.065	0.636	0.025	0.140	0.006
16518	R	21:33:32.53	-00:47:44.36	16.345	-17.8	10.4	0.301	0.063	1.072	0.080	0.445	0.023	0.086	0.006
03285	B	21:33:22.72	-00:51:43.29	16.745	-0.8	15.4	-0.420	0.020	0.934	0.033	0.367	0.023	0.060	0.006
04837	B	21:33:25.46	-00:51:11.67	16.316	-17.7	8.1	-0.395	0.016	0.980	0.025	0.388	0.023	0.054	0.006
11073	B	21:33:19.93	-00:49:20.21	16.021	-13.3	9.4	-0.127	0.071	0.891	0.117	0.394	0.023	0.054	0.006
14279	B	21:33:23.09	-00:48:25.03	16.206	18.3	6.8	-0.182	0.019	0.967	0.027	0.390	0.023	0.069	0.006
15906	B	21:33:20.10	-00:47:55.92	15.863	-10.0	8.3	-0.079	0.018	0.931	0.030	0.395	0.023	0.056	0.006
18369	B	21:33:22.04	-00:47:06.84	15.944	-6.7	7.5	-0.404	0.018	0.951	0.035	0.388	0.023	0.069	0.006
20166	B	21:33:23.46	-00:46:23.85	15.845	-5.7	7.7	-0.095	0.017	0.948	0.024	0.381	0.023	0.076	0.006
11876	B	21:33:22.42	-00:49:06.09	15.859	12.1	9.6	-0.138	0.018	0.870	0.030	0.384	0.023	0.069	0.006
04087	NM	21:33:14.53	-00:51:26.07	14.800	-48.5	12.2
17531	NM	21:33:30.33	-00:47:24.12	15.278	-60.3	5.8
19000	NM	21:33:36.69	-00:46:53.30	16.748	-81.6	9.4

^a ID is star ID number from Lardo et al. (2012b) photometric catalog.

^b Stars are defined B or R according to their location on the B- or R-RGB, respectively, in Figure 3. We flag M 2 non-member stars with NM.

VandenBerg 2001). The microturbulent velocity was determined using $v_t = -8.6 \times 10^{-4} T_{\text{eff}} + 5.6$, adopted from the analysis by Pilachowski et al. (1996) of metal-poor subgiant and giant stars with comparable stellar parameters. Table 2 reports the T_{eff} , $\log g$ and v_t values and their uncertainties; these values are used to choose the atmospheric model for the spectral synthesis of each star.

4.2 Abundances derivation and error analysis

Synthetic spectra were generated using the local thermodynamic equilibrium (LTE) program MOOG (Snedden 1973). The atomic and molecular line lists were taken from the latest Kurucz compilation (Castelli & Hubrig 2004) and downloaded from F. Castelli's website¹⁴. Model atmospheres were calculated with the ATLAS9 code starting from the grid of models available in F. Castelli's website (Castelli & Kurucz 2003), using the values of T_{eff} , $\log g$, and v_t determined as explained in the previous section and listed in Table 2. For all the models we adopted $[A/H] = -1.5$, according to the metallicity of the cluster. The ATLAS9 models employed were computed with the new set of opacity distribution functions (Castelli & Kurucz 2003) and excluding approximate overshooting in calculating the convective flux.

C and N abundances were estimated by spectral synthesis of the CH band at ~ 4310 Å and the NH and CN bands at 3360 and 3883 Å, respectively.

Figure 4 compares the N abundances derived from the NH and CN molecular bands. The correlation is very good and the difference between the two determinations is always within the errors. Therefore we considered in the following the *average* nitrogen abundances obtained from the NH and CN molecular bands. For the CH transitions, the $\log g_f$ obtained from the Kurucz database were revised downward by 0.3 dex to better reproduce the solar-flux spectrum by Neckel & Labs (1984) with the C abundance by Caffau et al. (2011), as discussed in Mucciarelli et al. (2012).

Finally, the Sr II 4077 Å and Ba II 4554 Å features were analyzed. The gf -values and solar abundances used for Sr and Ba are the same listed in Stanford et al. (2007).

In Figure 1 we show two representative B- and R-GB stars spectra (gray and black color, respectively) in the NH, CN, CH, Sr II and Ba II spectral regions.

An error analysis was performed by varying the temperature, gravity, metallicity, and microturbulence, and re-determining the abundances for three representative stars. Typically for the temperature, we found $\delta A(\text{C}) / \delta T_{\text{eff}} \simeq 0.09 - 0.11$ dex and $\delta A(\text{N}) / \delta T_{\text{eff}} \simeq 0.13 - 0.15$ dex. The errors in abundances due to uncertainties on gravity and microturbulent velocity are negligible (on the order of 0.02 dex or less). We also assumed that all stars had the same oxygen abundance ($[\text{O}/\text{Fe}] = +0.4$ dex) regardless of luminosity. The derived C abundance is thus dependent on the O abundance. To quantify the sensitivity of the C abundance on the adopted O abundance we varied the oxygen abundances and repeated the spectrum synthesis to determine the exact dependence for three representative stars ($4900 \text{ K} \leq T_{\text{eff}} \leq 5200 \text{ K}$). We found that variations in the oxygen abundance

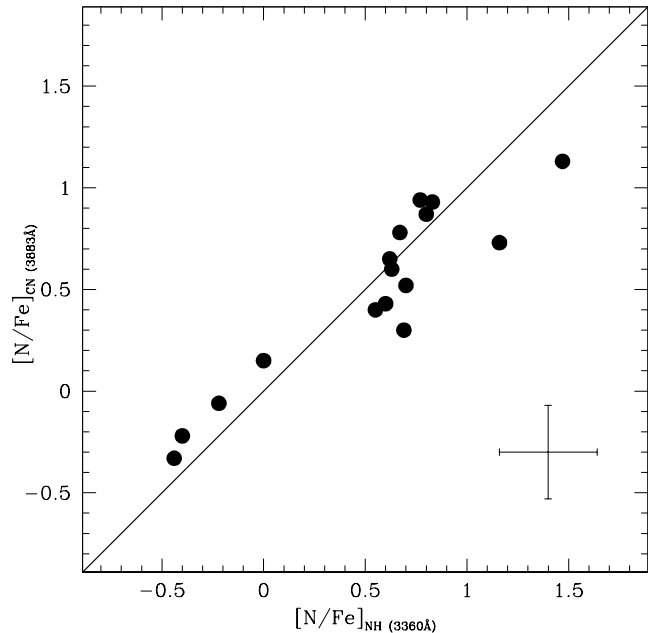


Figure 4. Comparison between the nitrogen abundances derived by synthesis of the NH band (~ 3360 Å) and those derived from the ultraviolet CN band at ~ 3883 Å. The 1:1 correlation line is also reported. Typical error bar on the measurements is also shown.

cause a variation in the derived $[\text{C}/\text{Fe}]$ by as much as $\simeq 0.10 - 0.11$ dex for a 0.4 dex change in assumed $[\text{O}/\text{Fe}]$. This error was then included in the final error of $[\text{C}/\text{Fe}]$.

All these individual errors were added in quadrature and gave a final error $\Delta[\text{C}/\text{Fe}] = 0.19$ dex, $\Delta[\text{N}/\text{Fe}] = 0.23$ dex. The uncertainties in Sr and Ba abundances were determined to be $\Delta[\text{Sr}/\text{Fe}] = 0.21$ dex and $\Delta[\text{Ba}/\text{Fe}] = 0.30$ dex.

We present the abundances derived as described above and the relative uncertainties in Table 2.

5 ABUNDANCE RESULTS

5.1 C-N anti-correlation

The derived carbon and nitrogen abundances are shown in Fig. 5, where the $[\text{C}/\text{Fe}]$ values are plotted as a function of $[\text{N}/\text{Fe}]$. In the same figure we plot also carbon and nitrogen abundances from DOLORES data derived in L12 with the $[\text{C}/\text{Fe}]-[\text{N}/\text{Fe}]$ relationship that prevails for these stars, to unambiguously identify the locus of the bulk of B-RGB stars in the $[\text{C}/\text{Fe}]$ vs. $[\text{N}/\text{Fe}]$ space¹⁵.

Having used the same analysis techniques, the two samples appear comparable (within the errors). Therefore in the following we discuss the MODS abundances together with DOLORES data presented in L12.

The newly derived C and N abundances for B-RGB stars coincide with the main C-N anti-correlation from DOLORES data, while R-RGB stars have, in general, higher

¹⁴ <http://wwwuser.oat.ts.astro.it/castelli/linelists.html>

¹⁵ We neglect stars brighter than the RGB bump because of evolutionary effects on C and N surface abundances which will be discussed in Section 5.3.

Table 2. Atmospheric parameters and C, N, Ba, and Sr abundance ratio for the M 2 cluster members.

ID	T (K)	eT (K)	log g (dex)	e log g (dex)	v_t (km/s)	ev_t (km/s)	[C/Fe] (dex)	e[C/Fe] (dex)	[N/Fe] (dex)	e[N/Fe] (dex)	[Sr/Fe] (dex)	e[Sr/Fe] (dex)	[Ba/Fe] (dex)	e[Ba/Fe] (dex)
05569	5136	59	2.5	0.03	1.3	0.4	-0.37	0.22	1.30	0.23	0.85	0.22	1.22	0.28
06893	5115	65	2.5	0.03	1.2	0.3	-0.24	0.18	0.61	0.25	0.45	0.23	1.15	0.30
08017	4868	67	2.2	0.03	1.4	0.5	-0.23	0.19	0.47	0.23	0.77	0.21	1.09	0.29
08984	4455	42	1.4	0.03	1.6	0.6	-0.99	0.20	0.51	0.22	0.81	0.21	1.12	0.31
10130	5019	55	2.5	0.03	1.3	0.4	-0.29	0.20	0.94	0.23	0.97	0.21	1.27	0.28
14911	4170	46	1.1	0.04	1.8	0.7	-0.93	0.19	0.07	0.23	0.53	0.22	0.88	0.28
16518	4833	51	2.3	0.03	1.4	0.5	-0.56	0.20	0.88	0.23	0.75	0.21	0.97	0.29
03285	5094	59	2.6	0.03	1.3	0.4	-0.49	0.19	-0.39	0.26	0.26	0.21	0.50	0.31
04837	5172	79	2.5	0.03	1.3	0.4	-0.63	0.18	-0.15	0.23	-0.12	0.22	0.34	0.30
11073	5095	78	2.3	0.03	1.3	0.4	-0.93	0.19	0.85	0.23	0.35	0.22	0.59	0.32
14279	5153	78	2.4	0.03	1.3	0.4	-0.52	0.19	0.72	0.23	0.25	0.22	0.57	0.35
15906	4962	73	2.2	0.03	1.4	0.5	-0.90	0.19	0.83	0.23	-0.10	0.21	0.52	0.29
18369	4955	73	2.2	0.03	1.4	0.5	-0.79	0.19	-0.31	0.23	0.15	0.21	0.33	0.30
20166	4910	72	2.2	0.03	1.4	0.5	-0.91	0.18	0.63	0.23	-0.04	0.21	0.66	0.27
11876	5180	60	2.3	0.03	1.3	0.4	-0.66	0.18	0.61	0.24	0.35	0.22	0.45	0.30

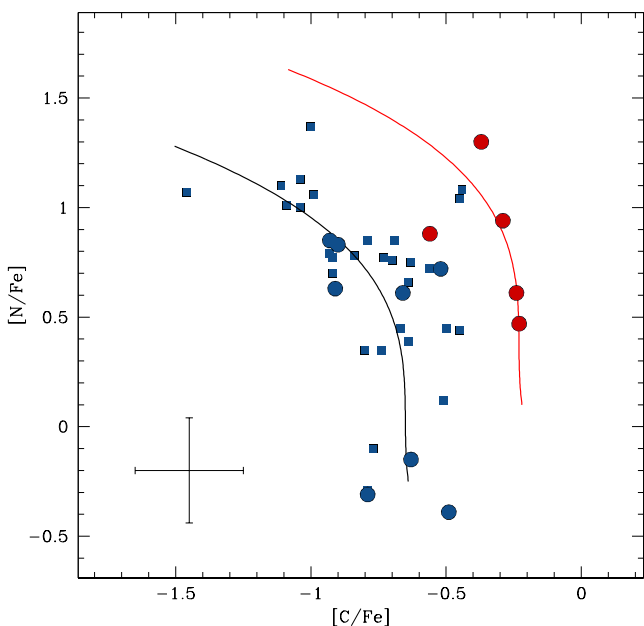


Figure 5. C and N anti-correlation for all the stars in the DOLORES and MODS sample. For readability purpose we report [C/Fe] and [N/Fe] abundance ratios only for stars fainter than the RGB bump. The black solid line indicate the relationship that prevails in B-RGB stars –with equation $[C/Fe] = -0.428 [N/Fe]^3 + 0.034 [N/Fe]^2 - 0.007 [N/Fe] - 0.650$. We shifted this fiducial line by $\Delta[C/Fe] = +0.42$ and $\Delta[N/Fe] = +0.35$ (red solid line) to visually fit the C-N anti-correlation showed by R-RGB stars. The symbols are the same as in Figure 3.

carbon abundances. We found that B-RGB stars have on average $[C/Fe] \simeq -0.77 \pm 0.14$ dex, that significantly differs from the average carbon content of the R-RGB populations ($[C/Fe] \simeq -0.29 \pm 0.06$ dex). Again, we noted a fully extended C-N anti-correlation for the B-RGB stars, while R-RGB stars tend to be richer in N, on average. Concerning the nitrogen abundances, we found an average value $[N/Fe] \simeq 0.75 \pm 0.20$ dex and $[N/Fe] \simeq 0.88 \pm 0.16$ dex for the B- and R-RGB population, respectively. Figure 5 suggests also that the R-RGB stars exhibit their own C-N anti-

correlation – although we are considering only five stars. The C-N pattern observed for the RGB stars recalls the Na-O anti-correlation analyzed for RGB stars in M 22 (Marino et al. 2009, 2011, 2012b), NGC 1851 (Yong & Grundahl 2008; Carretta et al. 2010b; Villanova et al. 2010) and ω Cen (Johnson & Pilachowski 2010; Marino et al. 2012a). Specifically, the blue and red RGB samples are not completely superimposed on one another in the [C/Fe]-[N/Fe] plane; while red RGB stars possibly show a shorter anti-correlation, with, on average, a higher nitrogen abundance (see also the behavior of faint and bright SGB stars in NGC 1851 shown in Figure 15 by Lardo et al. 2012a).

As discussed in L12, M 2 contains two CH stars (see Zinn 1981 and Smith & Mateo 1990). These stars show abnormally high CH absorption, together with deep CN bands, compared to other cluster giants. In our previous work on RGB stars in M 2, we confirmed that both CH stars belong to the additional RGB, pointing out the anomalous chemical nature of this redder branch. With the present analysis we are able to demonstrate that indeed R-RGB stars are C and N enhanced with respect to B-RGB ones.

5.2 Some comments on the C+N+O sum

Cassisi et al. (2008) and Ventura et al. (2009) argued that the SGB split of NGC 1851 can be accounted for by a difference in the overall CNO abundance between the two SGB groups without assuming a large age difference. Indeed, Yong et al. (2009) found evidence for strong CNO variations in a sample of four luminous RGB stars (but see the result of Villanova et al. 2010). In Lardo et al. (2012a) we analyzed the C+N sum for SGB stars NGC 1851 and measured a difference in $\log \epsilon(C+N)$ of 0.4 between the two SGBs, that implies that the fainter SGB has about 2.5 times the C+N content of the brighter one¹⁶.

In M 22 the faint SGB stars are enriched in *s*-process

¹⁶ However, we did not measure [O/Fe] abundances for our SGB stars and cautioned that the separation one sees in C+N content could significantly decrease or disappear when considering the C+N+O sum.

elements and additionally in the total C+N+O and metallicity Marino et al. (2012b). By accounting for the chemical content of the double SGB, these authors found that these two SGB groups do not differ in age by more than $\simeq 300$ Myr.

To investigate the possibility that the split SGB and the double RGB in M 2 could be due to a different C+N+O content between the two subpopulations, we computed the C+N sum for our B- and R-*RGB* stars. In the upper panels of Figure 6, we plot the generalized histograms of the C+N distribution for the MODS dataset considering the two *RGBs* separately¹⁷. The average C+N content of the two *RGB* populations is different: the R-*RGB* has $\log \epsilon(\text{C} + \text{N}) \simeq 7.35 \pm 0.25$ and the B-*RGB* has $\log \epsilon(\text{C} + \text{N}) \simeq 6.93 \pm 0.35$. When considering also the DOLORES sample, we established that the small difference in the total C+N+O content is slightly diminished; in this case the B-*RGB* has $\log \epsilon(\text{C} + \text{N}) \simeq 7.12 \pm 0.33$ (top right-hand panel of Figure 6).

Assuming an N-O anti-correlation, N-poor (first generation) stars in each *RGB* group are more O-rich than the N-rich (second generation) stars¹⁸. Even though we cannot measure oxygen abundances for our *RGB* stars, we can speculate on the C+N+O sum for the two *RGB* components assuming reasonable [O/Fe] value. As mentioned in Sect. 1 no oxygen abundance determination of M 2 *RGB* stars can be found in the literature, therefore we took as reference [O/Fe] values those derived by Marino et al. (2011) in the case of M 22, a cluster with similar metallicity ([Fe/H] = -1.70; Harris 1996, 2010 edition). The latter authors presented [C/Fe], [N/Fe], [Na/Fe] and [O/Fe] abundances for a number of *RGB* stars in M 22 located on both the red and blue *RGB* in M 22. Firstly, we note from their Figure 16 that also in that case each *RGB* displays its own C-N anticorrelation, with red *RGB* stars also having an excess of nitrogen. Second, again from their Figure 16, we derived a reference [O/Fe] abundance for N-poor and N-rich stars. We caution readers that assigning a reference [O/Fe] content to each group could be naïve at this stage¹⁹. If we assume for the N-poor and N-rich group [O/Fe] = 0.4 dex and [O/Fe] = 0.0 dex, respectively, the separation one sees in C+N content is largely diminished when considering C+N+O (right panels of Figure 6). We found that the R-*RGB* have $\log \epsilon(\text{C} + \text{N} + \text{O}) \simeq 7.69 \pm 0.13$ and the B-*RGB* $\log \epsilon(\text{C} + \text{N} + \text{O}) \simeq 7.59 \pm 0.10$ and 7.65 ± 0.10 – when considering only MODS and the entire sample, respectively. This exercise is not conclusive, of course, and new data on oxygen are badly needed, but it shows that if the analogy between M 2 and M 22 holds, the C+N+O sum in M 2 could change by a small amount, and age could play a rôle.

¹⁷ Each data point in these histograms has been replaced by a Gaussian of unit area and a standard deviation $\sigma=0.30$, the typical error associated to the measurements.

¹⁸ In the following, we arbitrarily discriminate between first and second generation stars by assuming a threshold in the nitrogen content [N/Fe] $\simeq 0.6$ dex.

¹⁹ Moreover, it is highly probable that oxygen abundance differences exist also between the R- and B-*RGB* stars.

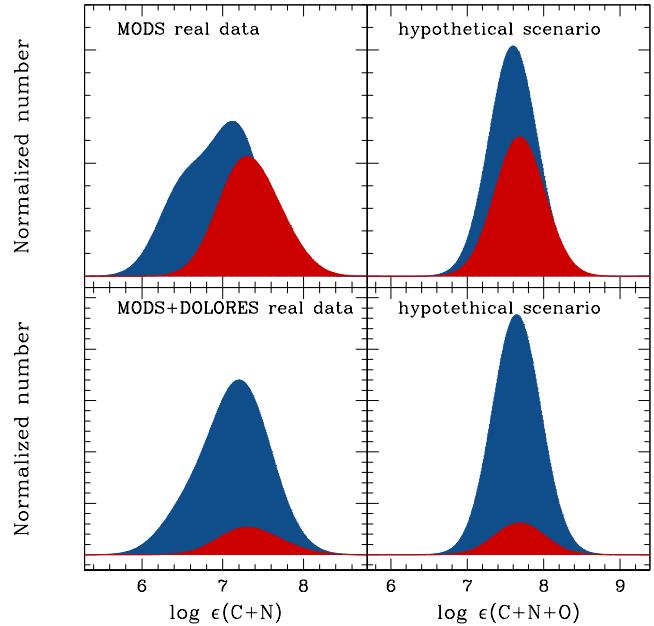


Figure 6. *Top:* on the left hand panel we reported the generalized histogram of the C+N distribution for MODS stars, flanked by the generalized histogram of the C+N+O distribution, obtained by assuming a reference [O/Fe] abundance for the N-rich and N-poor stars (see text). *Bottom:* the same as in the top panels but for the entire spectroscopic sample (DOLORES + MODS).

5.3 Evolutionary effects

In Figure 7 we plot the derived abundances against the temperature of stars to evaluate systematic effects with luminosity (and temperature) and note that neither of these effects are apparent. Once again we discriminated between stars fainter and brighter than the *RGB* bump, as significant CNO surface abundance changes are not expected to occur in stars fainter than the *RGB* bump (Iben 1968). While the Sr and Ba abundances of the R-*RGB* group are left unchanged as the stars evolve toward brighter luminosities, Figure 7 illustrates the notable depletion in the carbon abundances with luminosity (Smith & Martell 2003; Gratton et al. 2000, and references therein). This implicates that some form of deep mixing (i. e., meridional circulation currents, turbulent diffusion or some similar processes; see Charbonnel 1995; Charbonnel & Do Nascimento 1998; Angelou et al. 2012, and references therein) must circulate material from the base of the convective envelope down into the CN(O)-burning region near the hydrogen burning shell. In L12, we noted that the decline in the carbon abundance approximately occurred at magnitude $V \simeq 15.7$ mag, which is essentially the location of the *RGB* bump in this cluster (see L12 for a discussion). Our new data fully confirm this finding. Restricting our sample to those giants fainter than the *RGB* bump, we derive an average C abundance of [C/Fe] = -0.83 ± 0.26 dex, while stars more luminous than the *RGB* bump have average carbon abundance of [C/Fe] = -1.23 ± 0.17 dex²⁰.

Conversely, we see no significant trend of the N abun-

²⁰ For comparison, in metal-poor field giants (Gratton et al. 2000) a drop of the surface ^{12}C abundance by about a factor 2.5, it is seen after this second mixing episode.

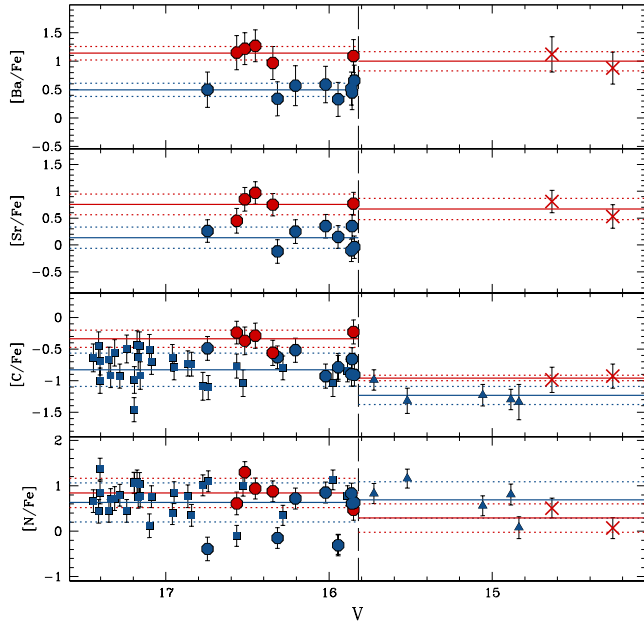


Figure 7. Run of the derived abundances with the temperature. The red (blue) horizontal line marks the position of the average abundance with the σ interval (dotted lines) for the R- (B-) RGB groups, respectively. The symbols are the same as in Figure 3.

dance with luminosity: the average nitrogen abundance we measure for stars fainter than the RGB bump ($[N/Fe] = 0.63 \pm 0.43$ dex) agrees quite well with that obtained for the more luminous stars after the RGB bump, $[N/Fe] = 0.56 \pm 0.38$ dex²¹. Gratton et al. (2000) show for field giants an abrupt increase in N abundance of about a factor of 4 at $\simeq V_{BUMP}$. Here, as in L12, we could not detect such trend. On the other hand, a few studies do not report a significant N enhancement for stars brighter than the RGB bump. Trefzger et al. (1983) studied a sample of 33 bright giants in M 15, a very metal poor cluster ($[Fe/H] = -2.37$, Harris 1996). They found that the mean carbon abundance declines with advancing evolutionary stage, but the mean N abundance does not change much along the RGB evolution. Carbon et al. (1982) found that the mean nitrogen abundance is essentially the same among subgiant and asymptotic giant branch stars in M 92. In the light of these results, a deeper investigation of N abundance changes along the RGB is needed. This goes beyond the scope of this paper.

5.4 s-process elements

Based on Figure 7, we note that Sr and Ba abundance values appear to be clustered around two distinct values for each RGB group. Confirming the results illustrated in Section 3, we found that R-RGB stars are enhanced in both Sr and Ba abundances with respect B-RGB stars. This appears immediately evident in Figure 1, where two representative B- and R-RGB stars are shown. These stars have essentially the same stellar parameters yet all these spectral features

²¹ We caution, however, that the extent of the carbon (nitrogen) depletion (enhancement) depends on the value of $[O/Fe]$ used in the analysis.

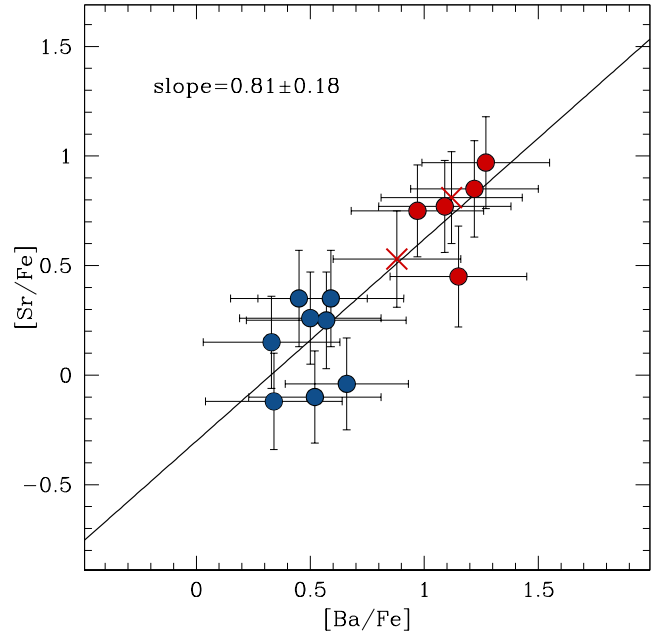


Figure 8. $[Ba/Fe]$ vs. $[Sr/Fe]$ abundance ratios are plotted with typical measurement uncertainties. The black line is the best least squares fitting straight lines. The symbols are the same as in Figure 3.

differ strongly²², the R-RGB stars clearly displaying strong NH, CN, and CH absorptions together with enhancement in the Sr and Ba abundances.

B-RGB stars have $[Sr/Fe] \simeq 0.25 \pm 0.19$ dex and $[Ba/Fe] \simeq 0.52 \pm 0.07$, that significantly differ from the average value found among the stars located on the R-RGB (for comparison $[Sr/Fe] \simeq 0.77 \pm 0.16$ and $[Ba/Fe] \simeq 1.12 \pm 0.12$ dex). To better visualize this result, in Figure 8, we show $[Ba/Fe]$ as a function of $[Sr/Fe]$, showing a clear correlation between these two s-process elements.

Figure 8 also shows that we can isolate a s-process element rich group and a s-process element poor one, each clearly corresponding to R- and B-RGB stars, respectively.

The bimodality in s-process elements found in M 2 clearly resembles the cases of NGC 1851 (Yong & Grundahl 2008; Villanova et al. 2010; Carretta et al. 2010b; Gratton et al. 2012) and M 22 (Marino et al. 2009; Da Costa & Marino 2011; Marino et al. 2011). Beyond the classical C-N and Na-O anti-correlations, these GCs display bimodal heavy element distribution and small metallicity spreads. Additionally, each s-group has its own C-N, Na-O anti-correlation (Carretta et al. 2010b; Villanova et al. 2010; Lardo et al. 2012a; Gratton et al. 2012; Marino et al. 2009, 2011, 2012b), suggesting that their star formation history must be more complicated than for the *normal* GCs. Interestingly enough, both clusters display a very complex CMD, with splits at the level of the RGB (Han et al. 2009; Carretta et al. 2011; Gratton et al. 2012; Marino et al. 2011) and SGB

²² Accidentally Figure 1 also confirms that the R-RGB star 05569 is a cluster member, because its spectrum is perfectly identical to that of the B-RGB star 04837 apart from the molecular features and the s-process element absorption lines.

(Milone et al. 2008; Piotto 2009; Lardo et al. 2012a; Piotto et al. 2012; Marino et al. 2012b).

6 SUMMARY AND CONCLUSIONS

We presented low resolution spectroscopy of 15 giants in M 2, located on the double RGB in $V, U - V$ diagram, with the goal to chemically characterize these two groups of RGB stars. We derived reliable abundances for four key elements – namely carbon, nitrogen, barium and strontium; thanks to the high quality of the MODS data.

As a first pass, we measured a set of spectral indices for all the observed stars. B-RGB stars have S3839 (CN band) indices comparable with those measured in our previous work (L12), while R-RGB stars have on average higher CN and CH absorptions. The higher resolution ($R@4000 \text{ \AA} \approx 1000$) of MODS spectra allowed us also to provide reliable index measurements for the Sr II $\lambda 4077$ and Ba II $\lambda 4554$ lines. We found that the R-RGB group has, in general, higher indices than the B-RGB one (see Figure 3).

Second, we used spectral synthesis to measure C, N, Ba and Sr abundances for all our stars. While B-RGB stars have carbon and nitrogen abundances well comparable to those derived from DOLORES data, R-RGB stars have enhanced [C/Fe] and [N/Fe] abundances (see Figure 5). Also, R-RGB giants show a hint of C-N anti-correlation. Moreover, we found that B- and R-RGB stars have different s -process element content (see Figure 8), R-RGB stars appearing systematically enhanced in both [Sr/Fe] and [Ba/Fe] than blue ones.

Finally, we conclude that this s -process bimodality along the RGB could be associated – as for M 22 and NGC 1851 – to the split SGB recently discovered by Piotto et al. (2012). Moreover, the R-RGB could tentatively be linked to the group of stars at the faint, blue end of the HB: the relative frequency on the R-/B- RGBs roughly matches the relative frequency of these blue HB stars with respect to the whole HB population ($\sim 5\%$ of stars, see also L12).

The general picture emerging from our analysis confirms that M 2 shows a strong resemblance to M 22 and NGC 1851, as speculated in L12. This assumption is mostly based on (i) the observed s -process element bimodality among RGB stars with the s -rich group having on average higher C and N abundances, (ii) the presence of a double RGB and (iii) a split SGB. Interestingly enough, both NGC 1851 and M 22 show a small spread in their iron content (Yong & Grundahl 2008; Carretta et al. 2010b; Gratton et al. 2012; Marino et al. 2012b). It would be of great interest to obtain high resolution spectra of it to investigate possible iron spread among M 2 RGB population.

As a final comment, we want to stress that with this study we identified as an additional RGB a group of stars that could easily be mistaken as field stars. Such situation could be more common than presently thought and a more careful inspection of U based CMDs is highly advisable. One of the obvious next steps would be to obtain carefully constructed CMDs – which include ultraviolet filters, for the GCs for which Piotto et al. (2012) reported the presence of a split SGB. Such RGB additional sequences, if observed

in other clusters, would present new challenges for multiple population studies.

7 ACKNOWLEDGEMENTS

We acknowledge the support from the LBT-Italian Coordination Facility for the execution of observations, data distribution and reduction. We thank the anonymous referee for a careful reading of the paper and helpful comments. This research has made use of the SIMBAD database, operated at CDS, Strasbourg, France and of NASA Astrophysical Data System.

REFERENCES

- Alonso A., Arribas S., Martínez-Roger C., 1999, *A&AS*, 140, 261
- Angelou G. C., Stancliffe R. J., Church R. P., Lattanzio J. C., Smith G. H., 2012, *ApJ*, 749, 128
- Armandroff T. E., Zinn R., 1988, *AJ*, 96, 92
- Bergbusch P. A., Vandenberg D. A., 2001, *ApJ*, 556, 322
- Bond H. E., 1975, *ApJL*, 202, L47
- Caffau E., Ludwig H.-G., Steffen M., Freytag B., Bonifacio P., 2011, *Sol. Phys.*, 268, 255
- Canterna R., Ferrall T., Harris W. E., 1982, *ApJ*, 258, 612
- Carbon D. F., Romanishin W., Langer G. E., Butler D., Kemper E., Trefzger C. F., Kraft R. P., Suntzeff N. B., 1982, *ApJS*, 49, 207
- Carretta E., Bragaglia A., Gratton R., D’Orazi D’Orazi V., Lucatello S., 2011, *A&A*, 535, A121
- Carretta E., Bragaglia A., Gratton R. G., Recio-Blanco A., Lucatello S., D’Orazi V., Cassisi S., 2010a, *A&A*, 516, A55
- Carretta E., Gratton R. G., Lucatello S., Bragaglia A., Catanzaro G., Leone F., Momany Y., D’Orazi V., Cassisi S., D’Antona F., Ortolani S., 2010b, *ApJL*, 722, L1
- Cassisi S., Salaris M., Pietrinferni A., Piotto G., Milone A. P., Bedin L. R., Anderson J., 2008, *ApJL*, 672, L115
- Castelli F., Hubrig S., 2004, *A&A*, 425, 263
- Castelli F., Kurucz R. L., 2003, in Piskunov N., Weiss W. W., Gray D. F., eds, *Modelling of Stellar Atmospheres Vol. 210 of IAU Symposium, New Grids of ATLAS9 Model Atmospheres*. p. 20P
- Charbonnel C., 1995, *ApJL*, 453, L41
- Charbonnel C., Do Nascimento Jr. J. D., 1998, *A&A*, 336, 915
- Cote P., Hanes D. A., McLaughlin D. E., Bridges T. J., Hesser J. E., Harris G. L. H., 1997, *ApJL*, 476, L15
- Da Costa G. S., Marino A. F., 2011, *Publication of the Astron. Soc. of Australia*, 28, 28
- Dalessandro E., Beccari G., Lanzoni B., Ferraro F. R., Schiavon R., Rood R. T., 2009, *ApJS*, 182, 509
- Dalessandro E., Salaris M., Ferraro F. R., Mucciarelli A., Cassisi S., 2013, *MNRAS*, 430, 459
- D’Antona, F., Caloi, V., Montalbán, J., Ventura, P., & Gratton, R. 2002, *A&A*, 395, 69
- D’Antona F., Bellazzini M., Caloi V., Pecci F. F., Galletti S., Rood R. T., 2005, *ApJ*, 631, 868
- Ferraro, F. R., Dalessandro, E., Mucciarelli, A., et al. 2009, *Nature*, 462, 483

- Girardi L., Groenewegen M. A. T., Hatziminaoglou E., da Costa L., 2005, *A&A*, 436, 895
- Gratton R., Sneden C., Carretta E., 2004, *ARA&A*, 42, 385
- Gratton R. G., Carretta E., Bragaglia A., 2012, *A&A Rev.*, 20, 50
- Gratton R. G., Sneden C., Carretta E., Bragaglia A., 2000, *A&A*, 354, 169
- Gratton R. G., Villanova S., Lucatello S., Sollima A., Geisler D., Carretta E., Cassisi S., Bragaglia A., 2012, *A&A*, 544, A12
- Han S.-I., Lee Y.-W., Joo S.-J., Sohn S. T., Yoon S.-J., Kim H.-S., Lee J.-W., 2009, *ApJL*, 707, L190
- Harding G. A., 1962, *The Observatory*, 82, 205
- Harris W. E., 1996, *AJ*, 112, 1487
- Hesser J. E., Bell R. A., Harris G. L. H., Cannon R. D., 1982, *AJ*, 87, 1470
- Iben Jr. I., 1968, *ApJ*, 154, 581
- Johnson C. I., Pilachowski C. A., 2010, *ApJ*, 722, 1373
- Kayser A., Hilker M., Grebel E. K., Willemsen P. G., 2008, *A&A*, 486, 437
- Kraft R. P., 1994, *PASP*, 106, 553
- Lardo C., Bellazzini M., Pancino E., Carretta E., Bragaglia A., Dalessandro E., 2011, *A&A*, 525, A114
- Lardo C., Milone A. P., Marino A. F., Mucciarelli A., Pancino E., Zoccali M., Rejkuba M., Carrera R., Gonzalez O., 2012a, *A&A*, 541, A141
- Lardo C., Pancino E., Mucciarelli A., Milone A. P., 2012b, *A&A*, 548, A107
- Lee J.-W., Carney B. W., 1999, *AJ*, 117, 2868
- Mackey A. D., van den Bergh S., 2005, *MNRAS*, 360, 631
- Marino A. F., Milone A. P., Piotto G., Cassisi S., D'Antona F., Anderson J., Aparicio A., Bedin L. R., Renzini A., Villanova S., 2012a, *ApJ*, 746, 14
- Marino A. F., Milone A. P., Piotto G., Villanova S., Bedin L. R., Bellini A., Renzini A., 2009, *A&A*, 505, 1099
- Marino A. F., Milone A. P., Sneden C., Bergemann M., Kraft R. P., Wallerstein G., Cassisi S., Aparicio A., Asplund M., Bedin R. L., Hilker M., Lind K., Momany Y., Piotto G., Roederer I. U., Stetson P. B., Zoccali M., 2012b, *A&A*, 541, A15
- Marino A. F., Sneden C., Kraft R. P., Wallerstein G., Norris J. E., da Costa G., Milone A. P., Ivans I. I., Gonzalez G., Fulbright J. P., Hilker M., Piotto G., Zoccali M., Stetson P. B., 2011, *A&A*, 532, A8
- Martell S. L., Smith G. H., 2009, *PASP*, 121, 577
- McClure R. D., Hesser J. E., 1981, *ApJ*, 246, 136
- McClure R. D., Norris J., 1977, *ApJL*, 217, L101
- Milone A. P., Bedin L. R., Piotto G., Anderson J., King I. R., SarAJedini A., Dotter A., Chaboyer B., Marín-Franch A., MAJewski S., Aparicio A., Hempel M., Paust N. E. Q., Reid I. N., Rosenberg A., Siegel M., 2008, *ApJ*, 673, 241
- Mucciarelli A., Salaris, M., & Bonifacio, P. 2012, *MNRAS*, 419, 2195
- Neckel H., Labs D., 1984, *solphys*, 90, 205
- Pancino E., Rejkuba M., Zoccali M., Carrera R., 2010, *A&A*, 524, A44
- Pilachowski C. A., Sneden C., Kraft R. P., 1996, *AJ*, 111, 1689
- Piotto G., 2009, in E. E. MamAJek, D. R. Soderblom, & R. F. G. Wyse ed., *IAU Symposium Vol. 258 of IAU Symposium*, Observations of multiple populations in star clusters. pp 233–244
- Piotto G., Milone A. P., Anderson J., Bedin L. R., Bellini A., Cassisi S., Marino A. F., Aparicio A., Nascimbene V., 2012, *ApJ*, 760, 39
- Robin, A. C., Reylé, C., Derrière, S., & Picaud, S. 2003, *A&A*, 409, 523
- Sharina M., Aringer B., Davoust E., Kniazev A. Y., Donzelli C. J., 2012, *MNRAS*, p. L503
- Smith G. H., Martell S. L., 2003, *PASP*, 115, 1211
- Smith G. H., Mateo M., 1990, *ApJ*, 353, 533
- Smith G. H., Norris J., 1982, *ApJ*, 254, 149
- Smolinski J. P., Martell S. L., Beers T. C., Lee Y. S., 2011, *AJ*, 142, 126
- Sneden C., 1973, *ApJ*, 184, 839
- Sneden, C., Kraft, R. P., Shetrone, M. D., et al. 1997, *AJ*, 114, 1964
- Stanford L. M., Da Costa G. S., Norris J. E., Cannon R. D., 2007, *ApJ*, 667, 911
- Trefzger D. V., Langer G. E., Carbon D. F., Suntzeff N. B., Kraft R. P., 1983, *ApJ*, 266, 144
- Ventura P., Caloi V., D'Antona F., Ferguson J., Milone A., Piotto G. P., 2009, *MNRAS*, 399, 934
- Villanova S., Geisler D., Piotto G., 2010, *ApJL*, 722, L18
- Vollmann K., Eversberg T., 2006, *Astronomische Nachrichten*, 327, 862
- Yong D., Grundahl F., 2008, *ApJL*, 672, L29
- Yong D., Grundahl F., D'Antona F., Karakas A. I., Lattanzio J. C., Norris J. E., 2009, *ApJL*, 695, L62
- Zinn R., 1981, *ApJ*, 251, 52